

Size of flux jumps in superconducting films

D. V. Shantsev,^{1,2} A. V. Bobyl,^{1,2} Y. M. Galperin,^{1,2} T. H. Johansen,^{1,3,*} and S. I. Lee^{4,5}

¹*Department of Physics, University of Oslo, P.O. Box 1048, Blindern, 0316 Oslo, Norway*

²*A. F. Ioffe Physico-Technical Institute, Polytekhnicheskaya 26, St. Petersburg 194021, Russia*

³*Texas Center for Superconductivity and Advanced Materials, University of Houston, Houston, Texas 77204-5002, USA*

⁴*National Creative Research Initiative Center for Superconductivity, Department of Physics, Pohang University of Science and Technology, Pohang 790-784, Korea*

⁵*Quantum Material laboratory, Korea Basic Science Institute, 52 Yeoeun-Dong, Yuseong-gu, Daejeon 305-333, Korea*

(Received 11 May 2005; published 26 July 2005)

Magneto-optical imaging is used to visualize vortex avalanches in MgB₂ films at 4 K. Avalanches ranging from 50 to 50 000 vortices were detected. The size distribution function has a clear peak whose position moves towards larger sizes as the applied field increases. This field dependence as well as variation of flux density profile during an avalanche is well described by a proposed model assuming a thermal origin of the avalanches. The model is based on the adiabatic approach and takes into account nonlocal electrodynamics in thin superconductors. The threshold field for thermal avalanches is predicted to be much smaller than that for thick superconductors, in agreement with the experiment.

DOI: 10.1103/PhysRevB.72.024541

PACS number(s): 74.25.Qt, 74.25.Ha, 74.78.Db, 74.70.Ad

I. INTRODUCTION

Applying a magnetic field to a type-II superconductor results in the formation of a metastable critical state with a nonuniform flux density, which is sustained by vortex pinning. From an application point of view the key quantity is the critical current density that determines the flux density gradient. However, much more information about the microscopic properties can be inferred from the time evolution of the critical state subjected to an external drive, e.g., a slowly increasing applied field. The repulsive interaction between individual vortices driven through a disordered pinning landscape may then result in avalanche dynamics, as already observed and analyzed in a number of experiments; see Ref. 1 for a review. Some studies^{2–8} have reported a power-law distribution of avalanche sizes, which is usually interpreted as a signature of self-organized criticality (SOC). However, in many experiments the distribution displays a peak at some preferred size^{4,5,8,9} or sometimes even two peaks.^{3,10,11}

These observations have motivated molecular dynamics simulations of the vortex motion, which predict a transition from a broad distribution to a peaked one as the density of pinning sites decreases.^{12,13} However, neither the simulations nor the SOC concept take into account thermal effects. It is well known that vortex motion generates heat, which makes pinning weaker and facilitates further motion. This positive feedback is responsible for large catastrophic vortex avalanches, or flux jumps,¹⁴ involving many millions of vortices, and usually causes heating of the superconductor to the critical temperature. To which degree also small-scale avalanches are affected by thermal effects is still very unclear and, hence, represents a major problem in understanding experimental results.

To be able to distinguish between avalanches of thermal and nonthermal origin one needs a clear theoretical prediction about the size of thermal avalanches. Previous theoretical studies of avalanche size considered slab superconductors placed in a parallel magnetic field.^{15,16} This geometry is dra-

matically different from that in most experiments where thin samples, often films, are placed in a perpendicular field. Therefore, the aim of this work is to (i) present a model that enables calculation of the size of flux avalanches in the perpendicular geometry and (ii) compare the predictions with experimental data obtained from magneto-optical (MO) imaging of flux dynamics in MgB₂ films.

We find that the avalanche size distribution, as well as the detailed variation of flux density profiles during an avalanche, is in good agreement with our model. It is shown that thermal flux jumps can be very small—down to 50 vortices—if the field is close to the threshold value.

II. FLUX-JUMP FIELD

Consider a thin superconducting strip with edges located at $x = \pm w$, thickness d , where $d \ll w$, and infinite in the y direction (see Fig. 1). When the zero-field-cooled strip is placed in a perpendicular magnetic field B_a , screening currents are induced the y direction. We shall assume the Bean critical state, i.e., $j = j_c$ in the flux penetrated region, j_c being the critical current density. Then the z component of flux density in the strip plane is^{17,18}

$$B(x) = B_c \ln \frac{x\sqrt{w^2 - a^2} + w\sqrt{x^2 - a^2}}{a\sqrt{w^2 - x^2}}, \quad a \leq |x| \leq w, \quad (1)$$

and $B(x) = 0$ in the central part of the strip, $|x| < a$. Here

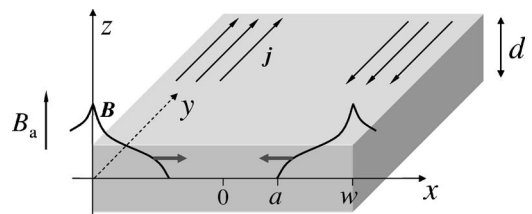


FIG. 1. Superconducting strip in a perpendicular magnetic field.

$$a = w/\cosh(B_a/B_c), \quad B_c = \mu_0 j_c d/\pi. \quad (2)$$

Let us assume now that a uniform fluctuation of temperature δT occurs. Assume also that the current-voltage curve of the superconductor is very steep near j_c , so that the induced flux motion proceeds faster than thermal diffusion. We can then use the adiabatic approach, i.e., assume that the heat stays where it is being released. The justification of this will be discussed in detail in Sec. V. The fluctuation leads to a decrease in the critical current density throughout the strip, by $\delta j_c = |\partial j_c / \partial T| \delta T$. Hence, some redistribution of flux density will occur, generating the Joule heat

$$\delta Q(x) = \int j E dt = j_c \int_a^x \delta B(x') dx', \quad x > a. \quad (3)$$

After substituting here Eq. (1) one obtains

$$\delta Q(x) = w B_c \left| \frac{\partial j_c(T)}{\partial T} \right| \gamma(x, B_a) \delta T, \quad (4)$$

with

$$\gamma(x, B_a) = \int_a^x \frac{B(x')}{B_c} \frac{dx'}{w} + \frac{\partial a}{\partial B_c} \int_a^x \frac{\partial B(x')}{\partial a} \frac{dx'}{w}. \quad (5)$$

Consider now the heat at the edge, since we expect this to be the most unstable region. The key quantity then is the ratio $\delta Q(w)/\delta T$, which should be compared with the specific heat C . If $C < \delta Q/\delta T$, the generated heat cannot be absorbed and the temperature fluctuation will grow. Thus, one finds that the superconductor is unstable if

$$\beta^{-1} < \gamma(w, B_a) = \frac{B_a}{B_c} \tanh \frac{B_a}{B_c} - \ln \left(\cosh \frac{B_a}{B_c} \right), \quad (6)$$

where

$$\beta^{-1} \equiv \frac{\pi C T^*}{\mu_0 d w j_c^2}, \quad T^* \equiv j_c \left| \frac{\partial j_c}{\partial T} \right|^{-1}. \quad (7)$$

The solution of Eq. (6) is shown graphically in Fig. 2 (top). The superconductor is stable if the applied field is below the so-called flux-jump field B_{fj} represented by a solid line. For small fields, $\gamma(w, B_a)$ grows parabolically as $\gamma \approx B_a^2/2B_c^2$, which allows us to find an explicit expression for the flux-jump field,

$$B_{fj} = \sqrt{2\mu_0 C T^*} \sqrt{\frac{d}{w\pi}}. \quad (8)$$

One can estimate from Fig. 2 (top) that this expression can be used for $B_{fj} < B_c$, or, as follows from Eq. (2), when the flux front penetrates less than 40% of the distance to the strip center. At high fields $\gamma(w, B_a)$ increases monotonically towards the asymptotic value of $\ln 2$. Therefore, in a strip flux jumps never happen if

$$\beta^{-1} > \ln 2. \quad (9)$$

It follows from Eq. (7) that β^{-1} is usually a monotonically increasing function of temperature since C grows with T , while j_c goes down. The temperature dependence of T^* gives

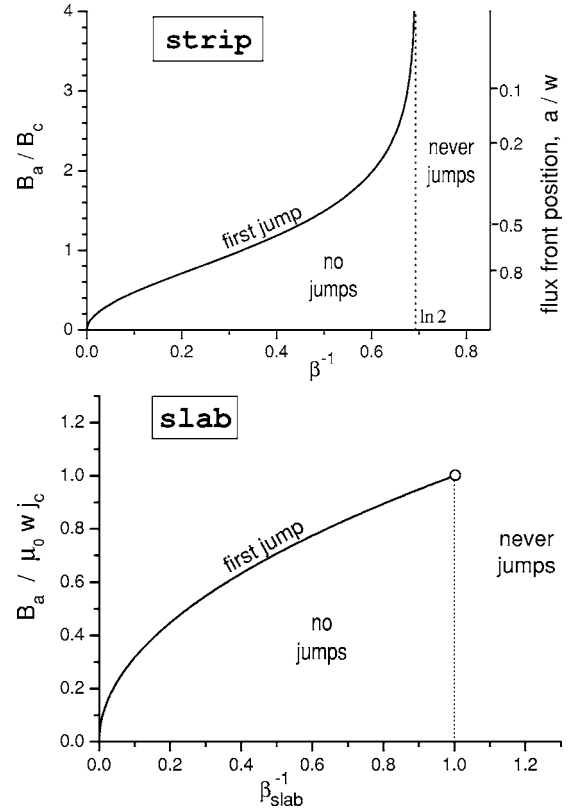


FIG. 2. Stability diagrams for a strip, Eq. (6), and for a slab, Eq. (11).

only a minor contribution possibly except for T very close to T_c . Figure 2 (top) can thus be considered as an approximation for the stability diagram in the B - T plane. It means that the condition (9) defines a threshold temperature above which flux jumps are not observed no matter how large a field is applied.

For comparison, let us recall the flux-jump criterion for a slab in a parallel field.^{15,16} This problem is much simpler since the field profiles are linear, and the result is that flux jumps in a slab of width $2w$ can happen only when

$$\frac{2CT^*}{\mu_0 w^2 j_c^2} \equiv \beta_{\text{slab}}^{-1} \leq 1 \quad (10)$$

and the flux jump field is

$$B_{fj}^{\text{slab}} = \mu_0 w j_c \sqrt{\beta_{\text{slab}}^{-1}} = \sqrt{2\mu_0 C T^*}. \quad (11)$$

The corresponding stability diagram is shown in Fig. 2 (bottom). It looks similar to that for a strip except for the existence of a well-defined point where the first-jump line ends. This difference stems from the fact that the applied field when the flux front reaches the middle of the sample, the full penetration field, is finite for a slab, but diverges for a thin strip.^{17,18}

Comparing Eq. (11) with the corresponding Eq. (8) for a strip one sees that the flux-jump field for a strip is smaller than that for a slab by a factor of $\sim \sqrt{d/w}$. It can be thought of as a “demagnetization factor” that characterizes the difference between the applied field B_a and the actual field at the

strip edge. This factor is essentially important since the aspect ratio of the strip d/w is of the order of 10^{-4} for most thin-film structures. Hence, thin films should be much more unstable with respect to flux jumps than bulk superconductors. The threshold temperature above which flux jumps are not observed should also be dramatically different for films and bulk samples. This is seen by comparing Eqs. (8) and (10) and noting that β is smaller than β_{slab} by a factor of $\sim d/w$.

III. JUMP SIZE

When the instability condition is met, any temperature fluctuation will trigger the development of a flux jump. In this section we will focus on the final state that the superconducting strip reaches after the jump. Using again the adiabatic approach, we find that the final temperature distribution $T(x)$ satisfies the following equation, which is obtained by integration of Eq. (3):

$$\int_{T_0}^{T(x)} \frac{C(T)dT}{j_c(T)} = \Phi(x). \quad (12)$$

Here T_0 is the initial temperature before the jump and

$$\Phi(x) = \int_0^x [B(x') - B_0(x')] dx' \quad (13)$$

is the flux per unit length that has passed through the point x during the whole course of the jump. $B_0(x)$ is the initial flux distribution. Again we employ the Bean critical-state model, so that $B_0(x)$ is given by Eq. (1) with $j_c = j_c(T_0)$. Similarly, in the final state one has $j(x) = j_c[T(x)]$ for all x where $B(x) \neq 0$. To complete the set of equations, the flux and current density distributions are connected via the Biot-Savart law

$$B(x) = B_a - \frac{\mu_0 d}{\pi} \int_0^w \frac{j(x')}{x^2 - x'^2} x' dx' \quad (14)$$

[where the symmetry $B(x) = B(-x)$ was taken into account].

In their solution of the analogous case of a slab in a parallel field Swartz and Bean¹⁵ called the final state after a flux jump the *adiabatic critical state*. The adiabatic critical state for a thin strip is therefore defined by Eqs. (12)–(14). We shall solve these equations numerically for the most commonly used T dependence of j_c and C , namely, the simple linear and cubic forms

$$j_c(T) = j_{c0}(1 - T/T_c), \quad C(T) = C(T_c)(T/T_c)^3. \quad (15)$$

Note that as the temperature increases during a jump, the heat capacity also grows, resulting in a stabilization of the flux jumps, thus limiting their size.

The solution of Eqs. (12)–(14) is not necessarily unique. To ensure that we find the proper one, we build the solution incrementally, simulating the evolution of the system during a flux jump. We start from a very small uniform temperature fluctuation δT and calculate the electric field $E \propto j(x) - j_c[T(x)]$ everywhere where $j > j_c$. The field and temperature variations are found as $\delta B = \delta E / \partial x$ and $\delta T = jE / C(T)$. Then

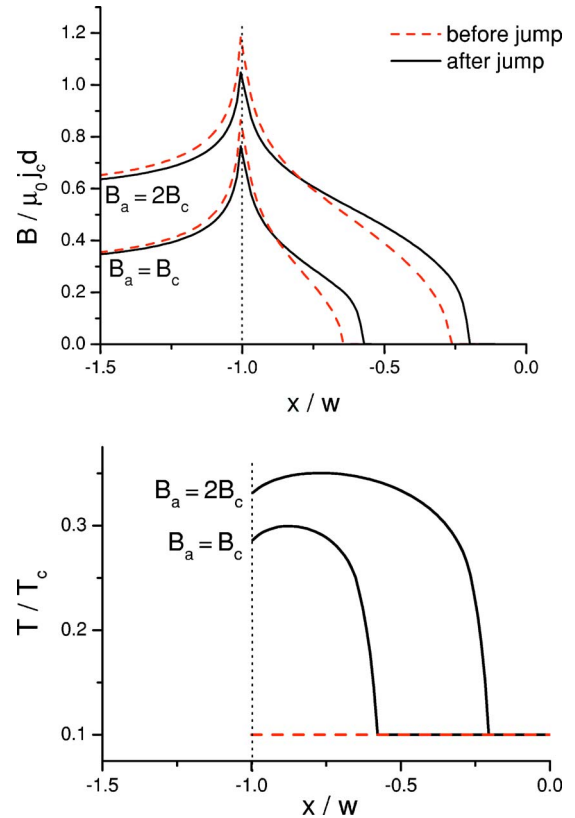


FIG. 3. (Color online) Flux density and temperature distributions before the jump (critical state, dashed lines) and after the jump (adiabatic critical state, solid lines) for two applied magnetic fields, where $\beta^{-1}(T_c/4) = \ln 2$ and $T = 0.1T_c$.

we recalculate E and continue until $j \leq j_c$ everywhere in the strip. The B and T distributions obtained by this procedure will satisfy Eqs. (12)–(14).

Shown in Fig. 3 are flux density and temperature profiles in the adiabatic critical state found by solving Eqs. (12)–(14). The flux profiles extend deeper into the strip than the initial critical-state profiles, which are shown by the dashed curves. The flux density $B(x)$ inside the superconductor has mainly increased, indicating penetration of additional flux into the strip during the jump. In a small region near the edge, and also on the outside, $B(x)$ has decreased in order to conserve the total amount of flux. The temperature has increased throughout the region where the flux motion took place. The single point where $B(x)$ did not change is obviously the point through which the maximum amount of flux $\Phi(x)$ has passed. Therefore it also shows the maximal temperature increase.

The jump size can be characterized by the total amount of flux arriving into the strip during the jump, $\Phi(w)$. Shown in Fig. 4 is $\Phi(w)$ plotted as a function of the applied field. For small B_a there are no jumps, in full agreement with the instability criterion, Eq. (6). As B_a increases above the threshold, the jump size grows too, eventually reaching a saturation value at high fields.

IV. EXPERIMENT

Flux jumps were studied in films of MgB₂ fabricated on Al₂O₃ substrates using pulsed laser deposition.¹⁹ The

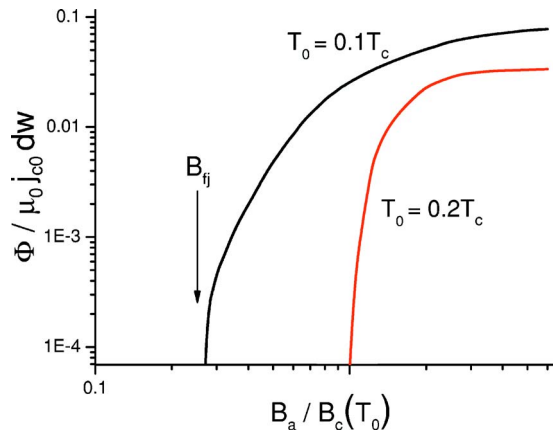


FIG. 4. (Color online) The flux-jump size as a function of applied magnetic field for $\beta^{-1}(T_c/4)=\ln 2$ and different T_0 .

samples had thickness of 400 nm and lateral dimensions $4.8 \times 4.8 \text{ mm}^2$. The films had a high degree of c -axis alignment perpendicular to the plane and showed a sharp superconducting transition at $T_c=39 \text{ K}$.

The flux density distribution was visualized using MO imaging based on the Faraday effect in ferrite garnet indicator films. For a recent review of the method, see Ref. 20, and a description of our setup is found elsewhere.²¹ The sample was glued with GE varnish to the cold finger of the optical cryostat, and a piece of MO indicator covering the sample area was placed loosely on top of the MgB_2 film. The grey levels in the MO images were converted to magnetic field values using a position-dependent calibration matrix.

Flux penetration was studied in zero-field-cooled films subjected to a slowly increasing perpendicular magnetic field B_a . The field ramp rate was chosen sufficiently slow, typically 0.01 mT/s, to give results that were rate independent. Shown in Fig. 5(a) is a MO image of a region near the film edge at $B_a=7.15 \text{ mT}$. The flux density is maximal at the film edge which is located near the bottom of the image. Most part of the film remains in the Meissner state which appears black on the image. The flux has here penetrated only a distance of $\sim 100 \mu\text{m}$ into film, and the flux front is seen to be strongly nonuniform. Such a nonuniformity is rather typical for superconducting films. It reflects the presence of defects at the edge that facilitate vortex entry.

To detect and quantify flux jumps we shall analyze difference images of the type shown in Figs. 5(b)–5(f). They are obtained by subtraction of subsequent MO images taken with 2-s intervals which implies $\Delta B_a=0.02 \text{ mT}$. The medium grey color here corresponds to unchanged flux density, while brighter areas show where B has increased. In all these images one can clearly see bright spots on the grey background and notice that their position always changes. These spots indicate flux jumps—an abrupt increase of flux density within a localized area. One can integrate the increase of flux density over the jump area to find the total amount of flux arrived there. E.g., for the jump shown in (g) it equals 900 flux quanta, while the average increase of B within the encircled region is 2.2 mT . The duration of one jump is shorter than 0.1 s since the human eye could not follow its evolution. We emphasize that shown in Figs. 5(b)–5(f) is not the

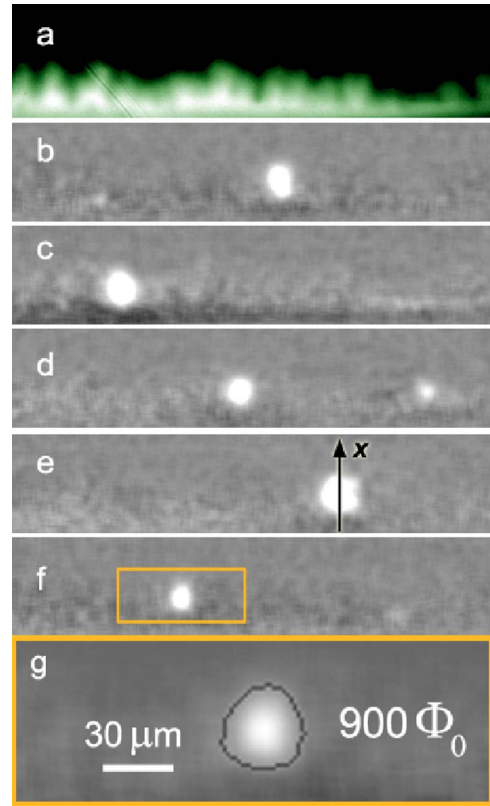


FIG. 5. (Color online) (a) MO image showing flux distribution near the edge of MgB_2 film for $B_a=7.15 \text{ mT}$ at 4 K. (b)–(f) Difference images obtained by subtracting two subsequent MO images taken with field interval $\Delta B_a=0.02 \text{ mT}$ display flux jumps (bright spots). (g) A blowup of the marked rectangular area on (f); the flux arrived within the outlined jump area is $900\Phi_0$, where $\Phi_0=h/2e$ is the flux quantum.

full series of difference images. Approximately 50% of images were omitted because they do not display any jumps.

Shown in Fig. 6 are profiles of flux density before and after flux jumps. They are recorded along the x axis perpendicular to the film edge, as shown in Fig. 5(e). The curves are very similar to the theoretical ones presented in Fig. 3 (top).

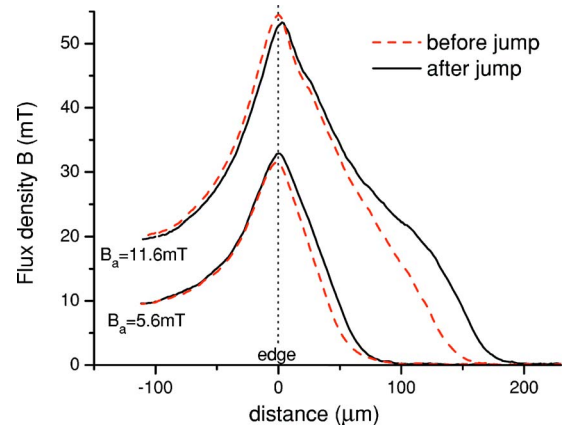


FIG. 6. (Color online) Profiles of flux density near the edge of MgB_2 film before and after a flux jump; the jump sizes are $7500\Phi_0$ for 5.6 mT and $31\,000\Phi_0$ for 11.6 mT .

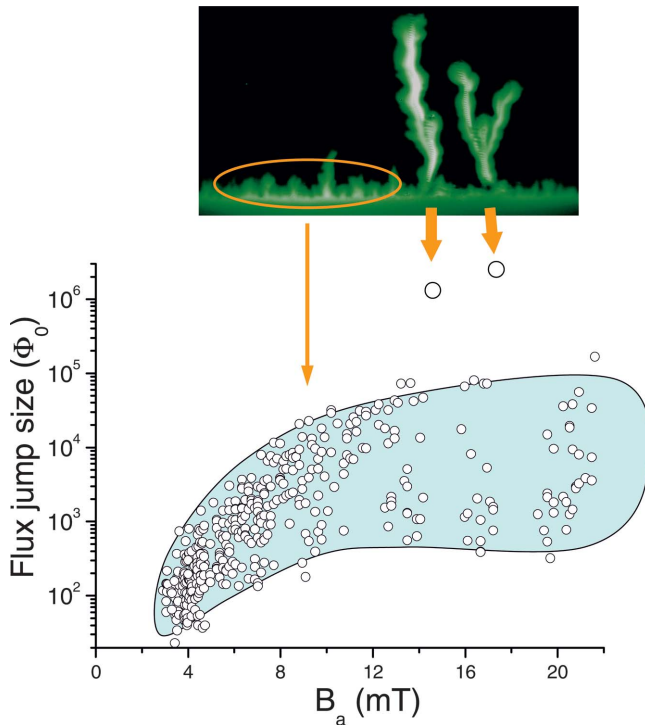


FIG. 7. (Color) Statistics of flux jump sizes in the MgB₂ film: every symbol corresponds to one jump.

Again we see an increase of B inside the film that is especially large close to the flux front and a slight decrease outside.

Let us now analyze quantitatively the size distribution of flux jumps. We ramped the applied field from zero to 23 mT at 3.6 K and kept a record of all flux jumps that took place within our observation window of 0.7 mm length along the film edge. The results are shown in Fig. 7 where every jump is represented by one symbol. The first jumps are detected around $B_a=3$ mT and are small, i.e., containing 100 or less vortices. As B_a increases, the average jump size steadily grows although with a large scatter of data. At $B_a=14.5$ mT we observed a jump of clearly different type. It is much larger than all the preceding jumps, extends on a distance of ~ 0.5 mm, and has a distinct fingerlike pattern. Another jump of the same type was observed at $B_a=17.5$ mT. Similar jumps, often called dendritic, have been reported earlier in films of MgB₂ (Refs. 22–24) and several other superconductors, in particular, YBa₂Cu₃O_{7-x},^{25,26} Nb,²⁷ Nb₃Sn,²⁸ YNi₂B₂C,²⁹ Pb,³⁰ and NbN.³¹ One sees from Fig. 7 that each dendritic jump is followed by an “empty” interval of B_a free of the small jumps. Obviously, such a massive flux intrusion significantly reduces the “magnetic pressure” on distances of the order of dendrite length. A considerable increase of applied field is then needed to build up this pressure again in order to trigger new jumps.

Apart from the region $B_a > 14$ mT affected by dendritic jumps, the observed $\Phi(B_a)$ dependence is in good agreement with the curve predicted for $T=0.1T_c$; see Fig. 4. Both the experimental and theoretical $\Phi(B_a)$ curves have a steep initial slope and tend to saturation at $B_a \sim 5B_{ff}$. Note that this qualitative agreement is achieved without any fitting param-

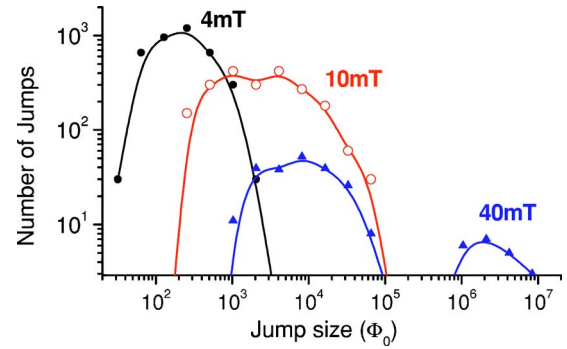


FIG. 8. (Color online) Flux-jump size distribution. The statistics are collected over all jumps that occurred in the MgB₂ film within 3-mT intervals of applied field centered around $B_a=4$, 10 and 40 mT.

eters. The only parameter in the model, β , is fixed by the experimental fact that the jumps do not occur above 10 K $\approx T_c/4$. Hence, according to Eq. (9), we have chosen $\beta^{-1}(T_c/4) = \ln 2$.

The large scatter of the measured jump sizes is probably due to sample inhomogeneities, which result in a very non-uniform penetration depth along the flux front, as seen in Fig. 5(a). Another factor increasing the scatter is the influence of preceding avalanches that can affect the initial state for the following flux jumps. To quantify the scatter of the jump sizes we collect statistics from the whole sample and plot the corresponding distribution functions in Fig. 8. The distribution strongly depends on the applied field B_a , as expected from Fig. 7. Although the distributions are rather broad, the increase of the average jump size as B_a changes from 4 to 10 mT is quite clear. Strictly speaking, the distribution function for $B_a=4$ mT might not be very accurate since we could have missed some jumps smaller than $50\Phi_0$ which is our resolution limit. However, for $B_a=10$ mT there is a definite peak in the range $(1000-4000)\Phi_0$. This rules out any possibility for SOC behavior characterized by a power-law size distribution. For larger B_a a distinct second peak appears in the size distribution due to dendritic avalanches.

To study the reproducibility of the observed jumps we carried out several identical experiments under exactly the same conditions. In order to visualize the difference between the flux distributions measured in three experiments, the three MO images were coded as red, blue, and green and then merged together; see Fig. 9 (top). The image appears almost perfectly black and white, demonstrating that the flux distribution is very reproducible from one experimental run to another. However, if one combines in a similar way three *difference* images, the resulting image is full of colors; see Fig. 9 (bottom). This means that the positions and sizes of flux jumps that took place as the applied field was increasing from 8.5 to 8.7 mT are not reproducible. For example, jump (a) occurred only in one experiment (green). Jump (b) occurred in all three experiments. However, its position and strength were not the same. It was the strongest in the “blue” experiment, but somehow weaker and shifted to the left in the “red” experiment and to the right in the “green” one. Only the jump (c) was fairly reproducible as seen by a purely

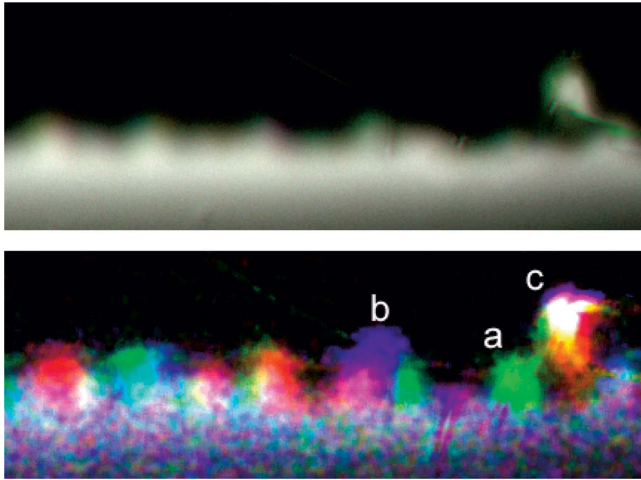


FIG. 9. (Color) Irreproducibility of flux jumps. Top: three MO images taken at $B_a=8.7$ mT in identical experiments are colored as red, blue, and green and merged together. Bottom: similar color merging for difference images that show flux jumps that took place between $B_a=8.5$ and 8.7 mT. Positions and sizes of flux jumps are unique for every experiment, though the final flux distribution is reproducible.

white region. In this case the place of the jump was predefined by a defect in the film. The presence of this defect can be immediately noticed by a reproducible peculiar feature in the flux distribution. We conclude therefore that in the absence of pronounced defects a unique and irreproducible sequence of flux jumps in every experiment produces a reproducible final flux distribution.

V. DISCUSSION

Most predictions of the proposed adiabatic model are in good agreement with the experimental results: namely, (i) the field dependence of the avalanche size, $\Phi(B_a)$ shown in Figs. 4 and 7, and (ii) the flux density profiles before and after a jump shown in Figs. 3 and 6. It suggests that the small vortex avalanches we observe in the MgB₂ film are of thermal origin. Another argument in favor of the thermal origin is the presence of huge dendritic jumps in the same film and in the same temperature range. The thermal origin of the dendritic jumps is now well established both experimentally (they are suppressed by contact with metal^{24,32}) and theoretically.^{22,33–36}

The coexistence of rather round and elongated dendritic jumps, both of thermal origin, can be understood within the recent theoretical models.^{33,34,36} They predict three possible situations depending on the parameters of the superconductor and the background electric field E : (i) stability, (ii) instability leading to uniform jumps, and (iii) instability leading to dendritic jumps. A transition from uniform to dendritic jumps should occur when E exceeds a threshold value. Experimentally, E is created by ramping the applied magnetic field and grows with B_a . Hence, the appearance of dendritic jumps at larger B_a seen in Fig. 7 perfectly agrees with the theories.³⁷

An important question now is whether the proposed adiabatic model predicting a jump size can be applicable to

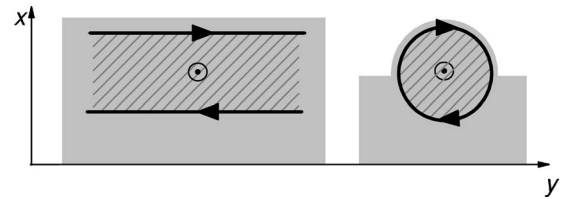


FIG. 10. Schematics of current redistribution during a uniform (left) and a round (right) flux jump. The flux penetrated area is grey, and the region where it has increased is hatched. Magnetic fields generated by two infinite wires (a) and by a current loop (b) differ only by a factor of $\pi/2$.

jumps of any shape. The model considered an ideal uniform film where a jump occurs uniformly along the flux front. The real sample is nonuniform, and the instability condition cannot be simultaneously met along the whole length of the front. Hence, every jump remains localized in the y direction and eventually acquires an approximately round shape or grows into a long dendrite. We made a rough estimate of the flux density increase due to current redistribution corresponding to a uniform and to a round jump schematically shown in Fig. 10. In the jump center the results are different only by a numerical factor of $\pi/2$. The resulting temperature rise is, in the adiabatic approach, determined only by the local flux motion and, hence, independent of the jump shape. This justifies the use of the proposed model to predict the size of round jumps. However, if a jump acquires a dendritic shape, the current distribution changes so significantly that the “uniform” model fails. Strong bending of the current flow around the jump area creates additional acceleration of the jump development. As a result, the size of dendritic jumps is usually limited only by the sample dimensions.

Our data show that the small jumps emerge as precursors of dendritic jumps when the applied magnetic field is increasing from zero. We believe that this is a general rule and that small jumps occur everywhere where dendritic jumps do. This explains the presence of two characteristic jump sizes reported in a number of experiments.^{3,10,11} On the other hand, one can imagine a situation when small flux jumps do occur, while the dendritic jumps do not. Then, even at very large applied fields there will be a special type of critical state which is formed by repeated local flux jumps. This was possibly the case in experiments on vortex avalanches where a peaked size distribution was measured.^{3–5,9,10}

The adiabatic approach used in our model implies that magnetic flux is moving faster than heat. This is very likely for the case of dendritic jumps where the flux is moving at velocities as high as 10–100 km/s.^{25,26} Moreover, the very fact that a jump acquires a dendritic shape implies, according to recent models,^{33,34,36} that the adiabatic approach holds. At the nucleation stage of flux jump the flux motion must be relatively slower, but even here the adiabatic approach seems to work well. Indeed, it predicts the flux jump field, Eq. (8), $B_{ff}=1.3$ mT in a reasonable agreement with experiment [for $C(4\text{ K})=0.3$ kJ/K m³ (Ref. 40)]. Had we been far from the adiabatic limit, the adiabatic model would have underestimated the flux jump field by a large ratio of thermal and magnetic diffusivities.^{14,39}

The total amount of flux that entered the strip during the field increase from 10 to 11 mT can be found by subtracting two corresponding MO images. This amount turns out to be 2 times larger than the sum over all flux jumps detected in the specified range of B_a . It means that only one-half of flux arrived into the superconductor via the flux jumps. The other half arrived via gradual penetration (or very small jumps that are below our resolution). This is not surprising. The adiabatic critical state established after every jump is characterized by less steep flux gradients than the original critical state. Therefore every jump should be followed by a relatively quiet period when increasing B_a results in a gradual penetration. The flux gradients build up during this period, bringing the system to the instability threshold again. We found that flux jumps in the same area occur with an interval of $\Delta B_a \approx 0.5$ mT.¹¹

Our analysis suggests that thermal flux jumps in superconducting films can be microscopic, down to at least 50 flux quanta. The thermal effects should therefore be carefully considered when analyzing the statistics of vortex avalanches even for small avalanche sizes. This is especially important

for Hall probe measurements that cannot access the spatial pattern of avalanches and always underestimate its actual size.

In conclusion, we propose an adiabatic model for flux jumps in thin superconductors. We find the flux and temperature distributions in the adiabatic critical state after a jump, the flux-jump field, and the threshold temperature above which jumps disappear. We find how the jump size depends on applied field and demonstrate, also experimentally, that thermal jumps can be virtually microscopic. In this sense they do not destroy the critical state, but instead provide the mechanism for its formation.

ACKNOWLEDGMENTS

The financial support by FUNMAT/UiO and the Research Council of Norway, Grant No. 158518/431 (NANOMAT), is gratefully acknowledged. The authors wish to thank E. Altshuler, R. Wijngaarden, and V. Vlasko-Vlasov for fruitful discussions and O. Shalaev for help.

*Electronic address: t.h.johansen@fys.uio.no

¹E. Altshuler and T. H. Johansen, *Rev. Mod. Phys.* **76**, 471 (2004).

²S. Field, J. Witt, F. Nori, and W. S. Ling, *Phys. Rev. Lett.* **74**, 1206 (1995).

³E. R. Nowak, O. W. Taylor, L. Liu, H. M. Jaeger, and T. I. Selinder, *Phys. Rev. B* **55**, 11702 (1997).

⁴K. Behnia, C. Capan, D. Mailly, and B. Etienne, *Phys. Rev. B* **61**, R3815 (2000).

⁵H. A. Radovan and R. J. Zieve, *Phys. Rev. B* **68**, 224509 (2003).

⁶C. M. Aegerter, M. S. Welling, and R. J. Wijngaarden, *Europhys. Lett.* **65**, 753 (2004).

⁷E. Altshuler, T. H. Johansen, Y. Paltiel, Peng Jin, K. E. Bassler, O. Ramos, G. F. Reiter, E. Zeldov, and C. W. Chu, *Phys. Rev. B* **70**, 140505(R) (2004).

⁸M. S. Welling, C. M. Aegerter, and R. J. Wijngaarden, cond-mat/0410369 (unpublished).

⁹R. J. Zieve, T. F. Rosenbaum, H. M. Jaeger, G. T. Seidler, G. W. Crabtree, and U. Welp, *Phys. Rev. B* **53**, 11849 (1996).

¹⁰S. S. James, S. B. Field, J. Siegel, and H. Shtrikman, *Physica C* **332**, 445 (2000).

¹¹A. V. Bobyl, D. V. Shantsev, Y. M. Galperin, A. A. F. Olsen, T. H. Johansen, W. N. Kang, and S. I. Lee, *Physica C* **408–410**, 508 (2004).

¹²O. Pla, N. K. Wilkin, and H. J. Jensen, *Europhys. Lett.* **33**, 297 (1996).

¹³C. J. Olson, C. Reichhardt, and F. Nori, *Phys. Rev. B* **56**, 6175 (1997).

¹⁴R. G. Mints and A. L. Rakhmanov, *Rev. Mod. Phys.* **53**, 551 (1981).

¹⁵P. S. Swartz and C. P. Bean, *J. Appl. Phys.* **39**, 4991 (1968).

¹⁶S. L. Wipf, *Phys. Rev.* **161**, 404 (1967).

¹⁷E. Zeldov, J. R. Clem, M. McElfresh, and M. Darwin, *Phys. Rev. B* **49**, 9802 (1994).

¹⁸E. H. Brandt and M. Indenbom, *Phys. Rev. B* **48**, 12893 (1993).

¹⁹W. N. Kang, H. J. Kim, E. M. Choi, C. U. Jung, and S. I. Lee, *Science* **292**, 1521 (2001).

²⁰Ch. Jooss, J. Albrecht, H. Kuhn, S. Leonhardt, and H. Kronmüller, *Rep. Prog. Phys.* **65**, 651 (2002).

²¹T. H. Johansen, M. Baziljevich, H. Bratsberg, Y. Galperin, P. E. Lindelof, Y. Shen, and P. Vase, *Phys. Rev. B* **54**, 16264 (1996).

²²T. H. Johansen, M. Baziljevich, D. V. Shantsev, P. E. Goa, Y. M. Galperin, W. N. Kang, H. J. Kim, E. M. Choi, M.-S. Kim, and S. I. Lee, *Europhys. Lett.* **59**, 599 (2002).

²³F. L. Barkov, D. V. Shantsev, T. H. Johansen, P. E. Goa, W. N. Kang, H. J. Kim, E. M. Choi, and S. I. Lee, *Phys. Rev. B* **67**, 064513 (2003).

²⁴M. Baziljevich, A. V. Bobyl, D. V. Shantsev, E. Altshuler, T. H. Johansen, and S. I. Lee, *Physica C* **369**, 93 (2002).

²⁵P. Leiderer, J. Boneberg, P. Brüll, V. Bujok, and S. Herminghaus, *Phys. Rev. Lett.* **71**, 2646 (1993).

²⁶U. Bolz, B. Biehler, D. Schmidt, B.-U. Runge, and P. Leiderer, *Europhys. Lett.* **64**, 517 (2003).

²⁷C. A. Duran, P. L. Gammel, R. E. Miller, and D. J. Bishop, *Phys. Rev. B* **52**, 75 (1995).

²⁸I. A. Rudnev, S. V. Antonenko, D. V. Shantsev, T. H. Johansen, and A. E. Primenko, *Cryogenics* **43**, 663 (2003).

²⁹S. C. Wimbush, B. Holzapfel, and Ch. Jooss, *J. Appl. Phys.* **96**, 3589 (2004).

³⁰M. Menghini, R. J. Wijngaarden, A. V. Silhanek, S. Raedts, and V. V. Moshchalkov, *Phys. Rev. B* **71**, 104506 (2005).

³¹I. A. Rudnev, D. V. Shantsev, T. H. Johansen, and A. E. Primenko, *Appl. Phys. Lett.* **87**, 042502 (2005).

³²E.-M. Choi, H.-S. Lee, H.-J. Kim, S.-I. Lee, H. J. Kim, and W. N. Kang, *Appl. Phys. Lett.* **84**, 82 (2004).

³³A. L. Rakhmanov, D. V. Shantsev, Y. M. Galperin, and T. H. Johansen, *Phys. Rev. B* **70**, 224502 (2004).

³⁴Igor S. Aranson, Alex Gurevich, Marco S. Welling, Rinke J. Wijngaarden, Vitalii K. Vlasko-Vlasov, Valerii M. Vinokur, and

- Ulrich Welp, Phys. Rev. Lett. **94**, 037002 (2005).
- ³⁵B. Biehler, B.-U. Runge, P. Leiderer, and R. G. Mints, cond-mat/0410030 (unpublished).
- ³⁶D. V. Denisov *et al.* (unpublished).
- ³⁷In real samples development of dendritic jumps can be hindered by nonuniformity of the flux front. Therefore another criterion can be of practical importance: a jump needs to exceed the typical scale of flux front roughness to get a chance to grow into a dendrite. This criterion is also in agreement with experiment because the jump size grows with B_d too.
- ³⁸R. G. Mints and E. H. Brandt, Phys. Rev. B **54**, 12421 (1996).
- ³⁹The flux-jump field for a thin strip found in Ref. 38 in the dynamic limit is much higher than that in the adiabatic limit found in this work.
- ⁴⁰Ch. Wälti, E. Felder, C. Degen, G. Wigger, R. Monnier, B. Dellely, and H. R. Ott, Phys. Rev. B **64**, 172515 (2001).